DOI: 10.13009/EUCASS2023-707
Aerospace Europe Conference 2023 – 10TH EUCASS – 9TH CEAS

Faraday Cup Design for Electrodeless Plasma Thrusters

Marco Riccardo Inchingolo⋆† *and Jaume Navarro-Cavallé*⋆
⋆*Equipo de Propulsión Espacial y Plasmas, Universidad Carlos III de Madrid*
Avenida de la Universidad 30, Leganés, Madrid 28911, Spain
minching@pa.uc3m.es · janavarr@ing.uc3m.es
†Corresponding author

Abstract

Faraday cups (FCs) are widely employed in electric propulsion to measure ion currents. In the case of electrodeless plasma thrusters, the typically lower ion energies and larger electron temperatures make it necessary to adopt additional care when designing and testing FCs. In this paper, the design of a FC is presented and the probe is used to scan the plume of a Helicon plasma thruster. A modular approach allows testing the effects of a set of design parameters on the collected ion current, namely two collimator types, the collector length, and collector material. Results show an ion current discrepancy of up to 50% between the probes equipped with the two collimators. However, no significant difference in the collected current is observed for the length and material studies, suggesting that secondary electrons generation or non-recollection are negligible in the ion energy and parametric range studied.

1. Introduction

Electrodeless plasma thrusters have gained significant attention in the field of electric propulsion due to their potential for longer thruster lifetime [1, 2]. In order to understand the characteristics of these thrusters and optimize their performance, diagnostic tools such as Faraday probes (FP), Langmuir Probes (LP), Retarding Potential Analysers (RPA), etc. have been extensively used.

Faraday probes allow for the measurement of ion currents in the plasma ejected by the thruster, biasing an electrode to negative voltages to reflect electrons and capture ions. Simply planar FP probes [3] commonly present problems related to sheath expansion and Secondary Electron Emission (SEE), furthermore they do not discriminate the ion velocity direction capturing ions from the whole probe field of view. Depending on the plasma properties, these individual effects are known to artificially increase the collected ion current, reducing the accuracy of the ion current determination, and consequently also on the thruster performance estimation. To compensate for these effects, different designs have been proposed in the literature. For example, the Guarded Faraday Probes help reduce the effect related to sheath expansion [4, 5, 6]. Among the other probe designs, the Faraday Cup (FC) configuration has emerged as a widely used approach. This probe is provided with a collimator and a cup-shaped collector enclosed in the probe casing helping respectively reducing the probe field of view and enhancing the recollection of SEE. Additionally, the expansion of the sheath with the bias voltage is contained within the probe, thereby preventing an undesired rise in the collected ion current [3]. Because of these advantages and versatility FCs are extensively used as a diagnostic tool in a variety of fields: nuclear physics [7], plasma sources [8, 9], and electric plasma thrusters. All of these, present different characteristics in terms of ion energy, densities, electron temperature, etc., parameters that must be taken into account for an effective probe design. We can find in the literature a wide range of studies and design optimization on FCs [10, 7, 8], however, the majority of these are in the keV ion energy range, hence with very different requirements with respect to electrodeless plasma thrusters. A significant contribution to FCs for electric propulsion has been made by Brown D., Mazouffre S., and Hugonnaud V.[4, 5, 3, 10, 11]. In their respective studies, they proposed various probe types and prototypes for measuring the plume of different thrusters, exploring variations in collimator shape, aperture size, collector size, and material properties. However, no clear probe design has emerged yet for the plasma properties typical of an electrodeless plasma thruster. For magnetic nozzle thrusters, in particular, the ion energies are typically in the same order of magnitude as the plasma potential at the ion current measurement location, this fact is expected to play a role in the ion optics determined by the geometrical constraints in the probe. Additionally, several aspects have not been assessed yet extensively concerning the role of SEE on the accuracy of the ion current measurements while working in these particular plasmas.

In this paper, we aim to address the role of several design parameters: the collimator size and shape and the collector length and material. To perform these studies, a modular FC design is proposed. Additionally, a segmented

DOI: 10.13009/EUCASS2023-707

collector is used to discriminate between the current collected at the lateral sides of the cup or at the back electrode. A Helicon thruster represents the source for the plasma under analysis, whose plasma properties are as well characterized by means of a LP and a RPA. Finally, this work provides some recommendations and guidelines or best practices for the use of FCs in the characterization of electrodeless plasma thrusters.

The rest of the paper is organized as follows. Firstly, the experimental setup employed for carrying out the experiment described in this study is outlined in Section 2, following, the Faraday Cup probe design is described extensively in Section 3.1. The plasma environment in which the FC probes are used is presented in Section 4.1 and finally the effect of the design alternatives is analyzed in Section 4. Lastly, Section 5 wraps up the work done and outlines best practices for FC use, and provide recommendations for optimal probe design in electrodeless plasma thruster diagnostics.

2. Experimental Setup

The plasma source used for the experiments of this work, is based on the thruster prototype described in Ref. [12] The helicon plasma thruster is operated at 13.56 MHz. The radio-frequency (RF) power is generated with a power amplifier, SerenHR2100, and fed to the thruster thanks to a custom-made matching network by Sener Aerospacial S.A [13]. The thruster has been operated at a constant power of $P_F = 350$ W, being P_F the forward power set by the amplifier, however, about 10% of this power will be lost in the transmission line. Power is coupled to the plasma through a half-helical silver-coated antenna wrapped around a quartz tube with a diameter $D_T = 25$ mm and 150 mm long. The magnetic field required for helicon coupling and the magnetic nozzle is produced with a single coil operated at $I_c = 12$ A, producing a magnetic field peak of about 600 G at its center. The thruster is operated between 5 and 20 sccm of Xenon, the mass flow rate being controlled by a Bronkhorst EL-FLOW select Xenon calibrated mass flow controller, with a resolution of 0.1 sccm and 100 sccm full range. The tests have been conducted inside the main vacuum chamber of the UC3M laboratory. It consists of a non-magnetic stainless-steel vessel of 1.5m inner diameter and 3.5m long. The vacuum is obtained through two turbo-molecular pumps, MAG2.200iP by Leybold, and three cryo-panels (COOLPOWER 140 T-V cryo-heads by Leybold). The facility background pressure is about 10^{-7} mbar, while the operating pressure is kept within the range 6 x 10^{-6}- 2.5 x 10^{-5} mbar for a Xe flow of 5 to 20 sccm. The thruster axis is aligned with the vacuum chamber axis, and the thruster outlet section is about 2.5 m away from the chamber downstream wall to minimize plume-chamber wall interactions.

Concerning the diagnostics setup, in this work, only electrostatic probes are used. Initial experiments were performed to characterize the plasma source, thus in addition to the Faraday Cups (FC), object of this study and discussed in detail in Section 3.1, two auxiliary probes are used for plasma characterization: a Retarding Potential Analyser (RPA, Impedance-Semion single button probe) and an RF compensated Langmuir Probe (LP). An additional description of the RF-compensated LP used in this work is available at Refs. [14, 15], for this test the Langmuir Probe tip electrode is 6 mm long, with a diameter of 0.256 mm. The data analysis and procedures of Ref. [16] are used to retrieve the plasma properties from the scanned data, i.e. I–V characteristic curve of a LP.

These two probes are mounted on a polar probe positioning system. This system is capable of moving probes on a plane along the radial ρ and polar α directions (Figure 1). The resolution of the system is about 0.3 mm and 1° for the radial and the polar directions respectively. The center of rotation of the probe positioning system is aligned with the center of the thruster exit plane. As discussed in Section 4.1, these probes are used to retrieve the plasma properties at a distance from the thruster of $\rho = 395$ mm and $\alpha = 0 - 60°$ where the ion current measurements are performed with the FCs.

DOI: 10.13009/EUCASS2023-707

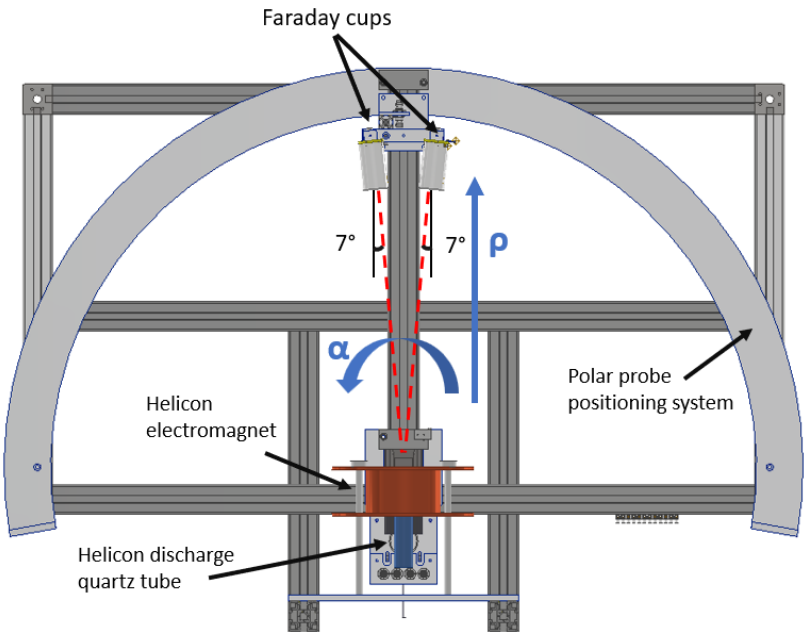

Figure 1: Setup assembly.

Two probe bodies and their internal components were manufactured. Having two probes in the same setup reduces the need for multiple experiment mounting iterations and allows for scans to be performed under the same thruster and plasma conditions for a more significant probe comparison. The Faraday Cups (FC) analyzed in this work are mounted by pairs in the same arm holder discussed above, as shown in Figure 1. The FCs are mounted symmetrically with respect to the radial direction at ρ = 395 mm, separated between each other by a distance of 96 mm and tilted by 7° so that the axis of the probes are pointing towards the thruster exit plane. However, due to this mounting strategy, only one probe is used at a time, so that the scan can happen for the same plume region.

3. Faraday Cup

3.1 Design

The modular FC design presented in this work allows varying easily the configuration of the internal components enabling the study of their importance on the collected current.

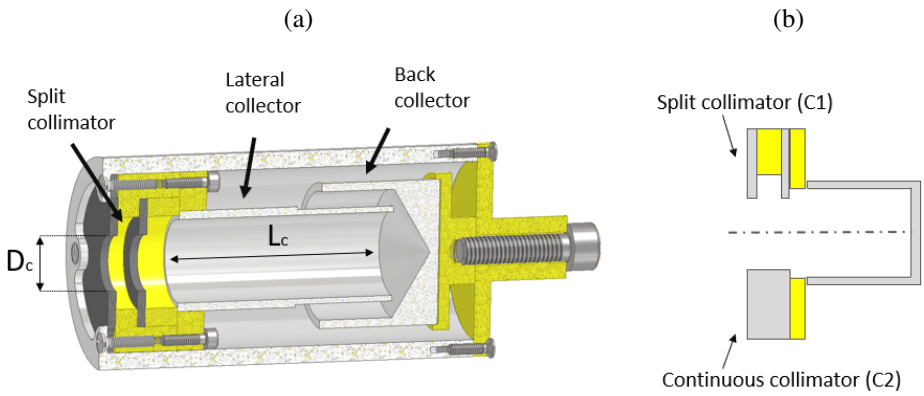

Figure 2: (a) CAD cut-view representation of the Faraday Cup probe design equipped with collimator C1. (b) Schematic drawing (not in scale) of the two collimator types in this study. Dielectric insulators (Teflon, PLA) are shown in yellow.

DOI: 10.13009/EUCASS2023-707

Figure 2-a shows a CAD cross-section view of the probe design. From the left to the right, one can see the collimator and the collector. Particles enter the probe through the collimator orifice. Once inside, because of the large negative biasing (V_b) of the collector, a non-neutral Child-Langmuir sheath is formed. Consequently, the resulting electric field attracts the ions, their charge is collected at the collector electrodes once in contact, supposing as well the recombination as neutral gas. In this design, the collector consists of an aluminum tube here called "lateral collector" and an additional "U" shaped electrode positioned at the back of the tube and referred to as "back collector". The diameter of the lateral collectors used in this work is 15 mm. In this work, two lengths for the lateral collector are tested L_c = 40 and 20 mm. Additionally, two back collector materials are also tested namely Aluminum and Tungsten HA195. Both electrode types are biased simultaneously at the bias V_b. This segmented collector design allows separating the contribution to the total collected ion current I_T in the lateral collector current, I_L, and in the back collector one I_B, so that $I_T = I_B + I_L$. Hence, using this design it is possible to obtain data providing a look into the ion current distribution inside the cup, which can be used as a useful tool for result interpretation as done in Section 4. The electrical connections to the FC collectors are realized with coaxial cables. The biasing voltage and the current measurement were obtained with a source-meter Keysight B2901A and a Keythley 6517B.

Conversely, in this study, two types of collimators are used, here defined as split (C1) and continuous (C2) collimators. A schematic view of C1 and C2 can be seen in Figure 2-b. Both C1 and C2 share the same hole diameter of D_c = 10 mm, defining an aperture area of $A_c = \pi D_c^2/4$ = 78.5 mm^2. C1 is composed of two conductive graphite disks with a thickness of 1.5 mm separated by a distance of 4 mm (Figure 2-a). C2 is a 10 mm long bored aluminum cylinder. Both of them are provided with an isolated electrical connection within the probe, making it possible to measure their floating potential and possibly apply an electrical bias.

The collimator defines the field of view (FoV) of the probe. The FoV can be described as the vertex of the cone in which an ion must be located to be collected by the probe. However, it is important to note that meeting this condition alone is not sufficient for collection. The orientation of the velocity vector of the ion also plays a significant role in determining whether it will be successfully collected by the probe. Ideally, a good Faraday Cup design would have the smallest field of view able to contain the thruster aperture, so that only the ions coming directly from the thruster and directed towards the FC would be collected.

The FoV of the probe equipped with C1 is 91.3° while for C2 it is 85°. Assuming ions travel only in straight lines, at each position in front of a Faraday Cup, only those within the allowed velocity vector range will be collected by the probe since they are in a collision course with the collector. The others will impact the collimator, casing, and dielectric components or not impact the FC at all. For each of these positions, one can define the maximum and minimum velocity vector angle (Θ_{max} and Θ_{min}) with respect to a reference (the probe axis for example) that would result in ion collection. Figure 3-a shows the $\Delta\Theta = |\Theta_{max} - \Theta_{min}|$ that allows ions collection at each position in the field of view of an FC equipped with C1.An example scheme is shown in Figure 3-b.

Figure 3-a shows that $\Delta\Theta$ grows approaching the probe (lower X), meaning that the FC would be able to collect those ions from that position with a larger disparity on their velocity vector direction (larger $\Delta\Theta$). Being D_c comparable to the thruster exit plane diameter D_T, placing the probe at closer distances would overestimate the ion current. This effect also becomes relevant in the presence of large amounts of CEX collisions with neutrals resulting in slow ions with a wider spread in velocity direction angle. [17, 18]. For this reason, the probes have been placed close to the farthest position allowed by the probe positioning system (395 mm from the thruster exit plane), as discussed in Section 2.

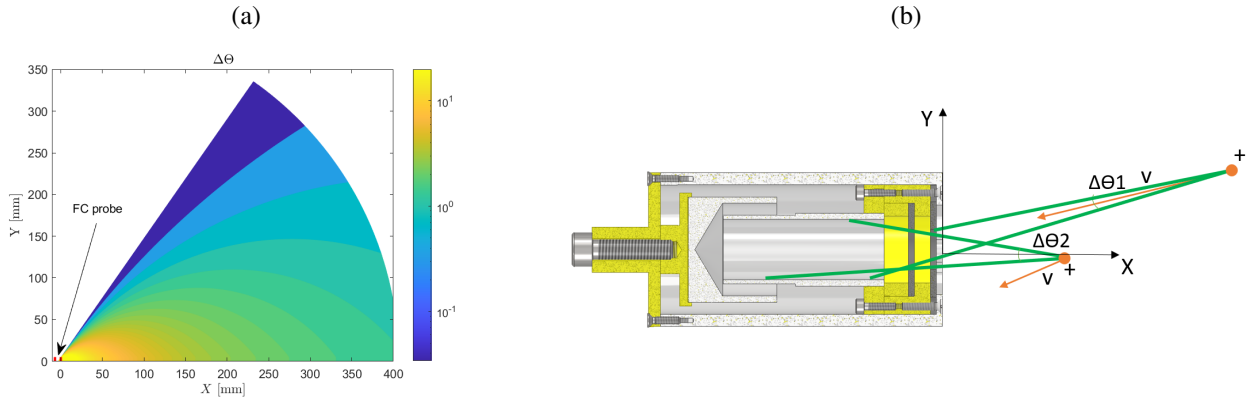

Figure 3: (a) $\Delta\Theta$ in the FoV cone of a probe equipped with collimator C1. (b) Scheme showing two ions with allowed/not-allowed velocity vector for FC probe ion current collection. XY are the FC body axes.

DOI: 10.13009/EUCASS2023-707

ID	Collimator type	Collector length (L_c)	Back collector material
FC-A	Split (C1)	4 cm	Aluminium
FC-B	Continuous (C2)	4 cm	Aluminium
FC-C	Split (C1)	2 cm	Aluminium
FC-D	Split (C1)	2 cm	Tungsten

Table 1: Table summarising the Faraday Cup design alternatives.

Finally, in this study, different design alternatives are proposed for the internal elements, their differences are summarized in table 1.

3.2 Operation and data post-processing

It is noteworthy to mention that, before the first use of the probe after assembling, an electrode cleaning procedure using electron bombardment has to be carried out. This allows for removing electrode surface impurities and obtaining reliable and consistent results: the probe is positioned in a region with higher density (ρ = 100 mm at 5 sccm), and both the lateral and back collector are biased to a high positive bias (typically V_b = 200 V). An example of the I-V characteristic curve collected before and after the cleaning procedure is shown in Figure 4.

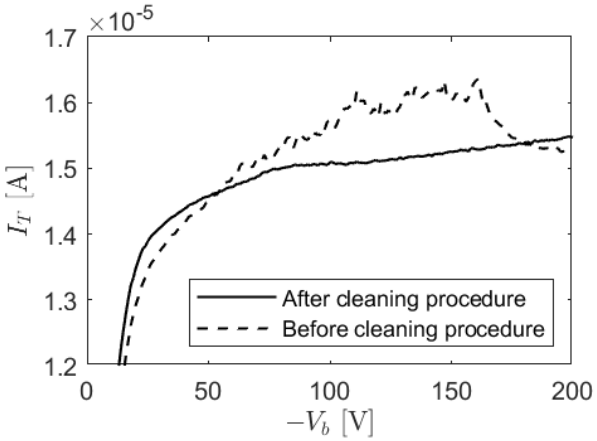

Figure 4: I-V curve collected by the Faraday Cup before and after the cleaning procedure.

Two types of FC scans are performed in this study, I-V curves and plume scans. The I-V curves are obtained by keeping the probe at the measurement location and sweeping the bias of the collector from $V_b = 0$ to high negative bias to enter the ion saturation region (typically $V_b = -130$ V or -200 V). The plume scans are performed at a fixed value of collector bias, $V_b = -100$ V since for this value the ion current is saturated for all the tested plasma conditions.

Assuming plume axisymmetry, and having measured the ion current density $j_i = I_T/A_{FC}$ at different angular positions α, it is possible to estimate integrated plume properties: the ion beam current, I_b, the utilization efficiency η_u and the plume divergence angle α_D. I_b is given by:

$$I_b = 2\pi\rho^2 \int_0^{\pi/2} j_i(\alpha)\sin(\alpha)\, d\alpha, \tag{1}$$

Assuming a singly-charged ion beam, the utilization efficiency is then defined as the (normalized) ratio between the ion beam current and the input mass flow rate,

$$\eta_u = \frac{\dot{m}_i}{\dot{m}_p} \simeq \frac{I_b m_{Xe}}{e\dot{m}_p}, \tag{2}$$

where $\dot{m}_i$ is the ion mass flow rate in the plume, e is the unit charge and m_{Xe} is the Xenon atomic mass. The divergence efficiency can be found considering the portion of current directed in the axial direction,

$$\eta_D = \frac{I_{i,ax}^2}{I_b^2}, \tag{3}$$

with $I_{i,ax} = 2\pi\rho^2 \int_0^{\pi/2} j_i(\alpha)\sin(\alpha)\cos(\alpha)\, d\alpha$.

DOI: 10.13009/EUCASS2023-707

4. Results

The influence of the design parameters on the ion current collection is here discussed. Firstly, in Section 4.1 the plasma environment is assessed with the help of a LP and a RPA. In Section 4.2, 4.3, and 4.4 the effect of the different tested collimators, collector length, and material are respectively analysed.

4.1 Plasma Environment and test conditions

Knowing the plasma conditions at the Faraday Cup location can provide insights into the cup's performance and help the result interpretation. Furthermore, the data provided in this Section are essential for a correct design of a FC as discussed in Section 3.1. As mentioned in Section 2 a Retarding Potential Analyzer (RPA) and a Langmuir probe (LP) were used as auxiliary probes. The analysis of the I-V curve from a LP provided the ion density n_i, the electron temperature T_e, and the plasma potential V_p. The RPA is used to determine the most probable total ion energy E_i (potential plus kinetic energy). The plasma properties were evaluated at the Faraday Cup probing position used for this experiment: $\rho = 395$ mm and $\alpha = 0 - 60°$.

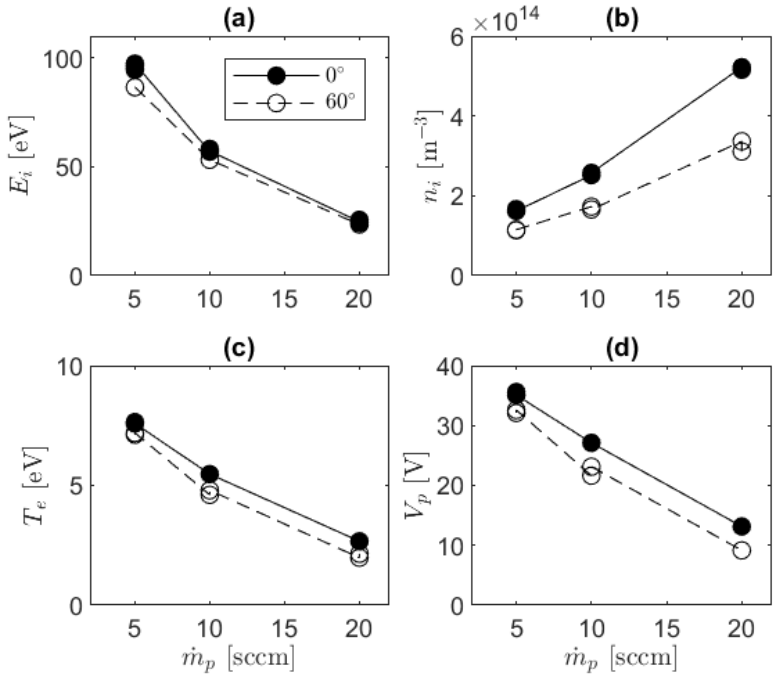

Figure 5: Plasma environment at the FC probe distance. (a) Most probable ion energy E_i according to the IEDF measured by the RPA. (b,c,d) ion density, electron temperature, and plasma potential from the LP I-V characteristic curve.

As typically happens for Helicon plasma thrusters and, in general, magnetic nozzle thrusters [19], increasing the mass flow rate reduces the available energy per electron, and simultaneously increases the electron collision rate. This lowers the electron temperature (refer to Figure 5-c), and consequently the potential drop available for the ions in the magnetic nozzle. Hence, E_i results are strongly dependent on the mass flow rate. Peak ion energies of about 100 eV were found on the axis (Figure 5). However, E_i is found to be weakly dependent on the angular position. From the data available in Figure 5, Debye lengths close to the one-millimeter range are expected to be found at these distances. Furthermore, the data provided can be used to obtain a useful order of magnitude for the ion current density j_i that the FC probes are expected to measure. j_i can be obtained as $j_i = n_i v_i e$, where v_i is the local ion velocity: $v_i = \sqrt{2(E_i - V_p)/m_{Xe}}$. Estimations of j_i provide values in the order of $0.15 - 0.35$ A/m^2, which as shown in the next section, is in line with the FC measurements.

DOI: 10.13009/EUCASS2023-707

4.2 Effect of the Collimator

Two different collimators have been tested: a split collimator (FC-A) and a continuous collimator (FC-B). Both designs share a similar geometrical view angle. The plume has been scanned at the probe nominal distance (ρ = 395 mm) with a fixed collector bias voltage of $V_b = -100$ V. The ion current density profiles obtained with the two collimator geometries are shown in Figure 6 together with the computed propellant utilization efficiency. Firstly, the current density levels reached on the axis result being very close to the ones estimated just using the LP and RPA data. This is particularly true for the FC-A case. The plume presents a peak in the center for all the mass flow rates tested, however, local maxima are developed at around $\alpha = \pm 50^\circ$ which tend to disappear as $\dot{m}_p$ is raised. This behavior is not yet completely understood, but it has been seen in other previous works [20]. One of the hypotheses is that a second less-magnetized beam forms in proximity to the discharge chamber walls, this might happen because of CEX collisions with the recombined ions at the walls.

The utilization and divergence efficiency have been estimated from these data, staying below 25% and 45% respectively. This result agrees with those presented in Section 4.1, rising the mass flow rate reduces the electron temperature resulting in a lower ionizing capability. On the other hand, the disappearance of the lateral peaks makes the divergence efficiency improve with $\dot{m}_p$.
The two probes recover the same profile shape, but the measured current level is different. The split collimator (FC-A) shows about 45-50% more current with respect to the continuous collimator probe (FC-B). Since the shape is preserved, the differences in the divergence estimation are small.

To understand how the collimator design affects the current collection, I-V curve scans have been measured on the plume axis (Figure 7). The segmented collector has been used as a diagnosing tool to investigate the source of this difference.

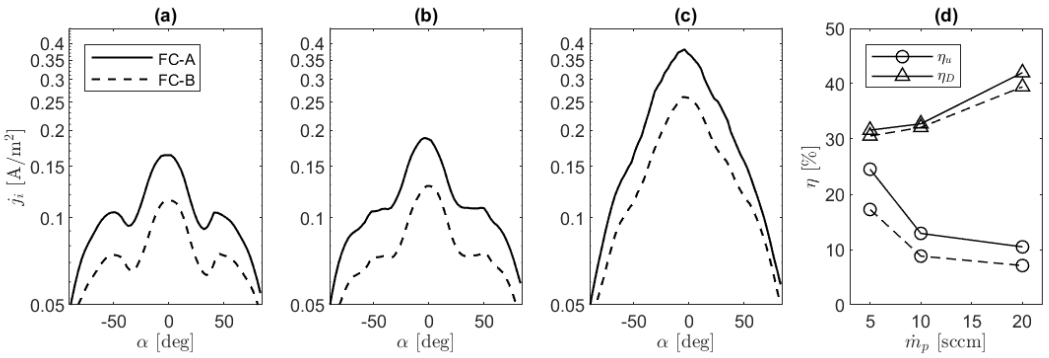

Figure 6: Plume scans with FC-A and FC-B for three different mass flow rates, $\dot{m}_p$ = 5 (a), 10 (b), and 20 (c) sccm. Panel (d) shows the propellant utilization efficiency η_u and the divergence efficiency η_D for the two probes at the different mass flow rates tested.

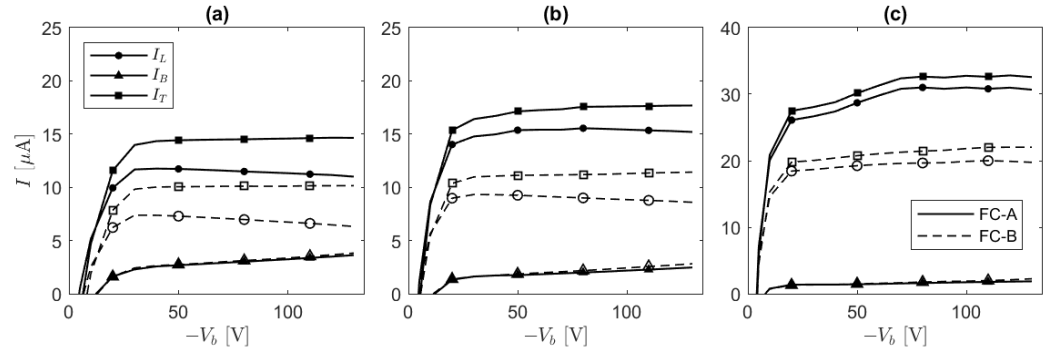

Figure 7: I-V curves for the probe with split collimator FC-A (solid lines) and continuous collimator FC-B (dashed lines) for $\dot{m}_p$ = 5 (a), 10 (b) and 20 sccm (c). All the curves are taken on the thruster axis.

DOI: 10.13009/EUCASS2023-707

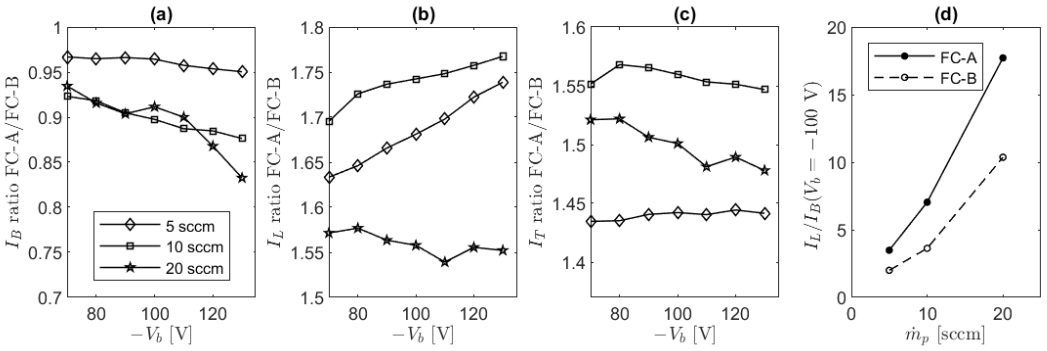

Figure 8: Collected current ratios I_B (a), I_L (b), $I_T(c)$ for $\dot{m}_p = 5$, 10 and 20 sccm. (d) ratio between the lateral and back current collected for FC-A (solid) and FC-B (dashed).

Figure 7 shows the I-V curves obtained for the back and lateral collector together with the total current as introduced in Section 3.1. The previously observed discrepancy in the total current can also be seen in the I-V curves. For a useful comparison, the ion currents shown in Figure 7, are displayed as ratios in Figure 8. I_B is weakly dependent on which type of collimator is used. I_B for the probe FC-A is less than 5% lower than the one for the FC-B case, this value increases with the mass flow rate and can reach up to 15% for 20 sccm (Figure 8-a). Thus, the greatest contribution to the total current discrepancy is brought by I_L, the probe using the split collimator collecting up to 75% more current (Figure 8-b). This is also the source for the lower I_L/I_B ratio shown by the FC-B.

Finally, understanding how much current reaches the lateral collector with respect to the back one, can provide clues on the ion trajectory inside the probe. Referring to Figure 8-d, the ratio of current I_L/I_B, increases with the mass flow rate, the value at 100 V was taken as reference. This effect must be related to the reduced ion energy with $\dot{m}_p$ as was shown in Figure 5-a, the lower energy makes it easier for the sheath on the lateral collector to deflect ions towards itself rather than letting them proceed in a straight line towards the back collector.

To understand the origin of the reduced current collected by the lateral collector, a simplified 1D sheath model on the C2 continuous collimator has been employed. The electrons are assumed Maxwellian and the ions to enter the sheath with the Bohm velocity. Considering ion energy conservation, the model solves the Poisson equation in the sheath along a floating planar surface parallel to the Z direction (here representing the C2 collimator surface). The floating condition is achieved by setting the ion and electron flux at the surface to be equal. The floating surface extends from $Z = 0$ mm to $Z = 10$ mm. The domain extends several times the Debye length in the perpendicular direction Y. Note that, being 1D, the model assumes the plasma properties to be constant along the Z direction and neglects any boundary effect around the margins of the floating surface. The resulting perpendicular electric field within the sheath (E_Y) is used to propagate the trajectory of ions incoming at different distances Y from the surface, and initially traveling along the Z direction with a kinetic energy of $E_k = E_i - V_p$ at $Z = 0$.

Figure 9 shows the resulting ion trajectories for the three tested plasma conditions at 5, 10, and 20 sccm. The electron temperature, ion energy and density required for the solution are those found experimentally and available

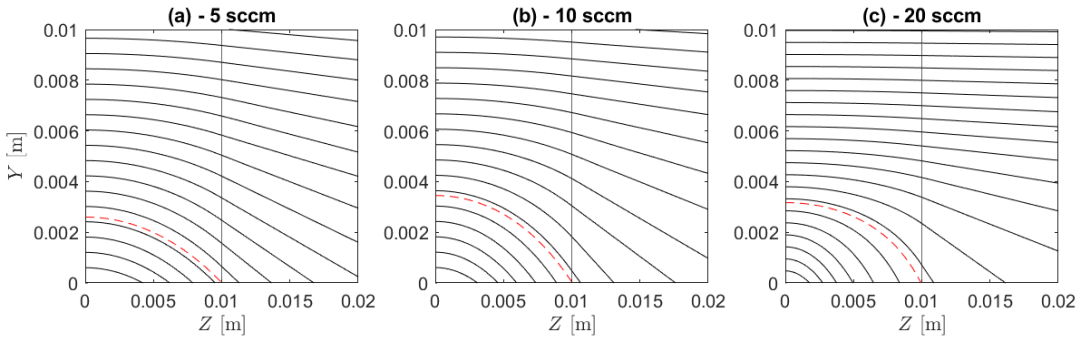

Figure 9: Ion trajectory along a floating surface ($Y = 0$ m) for the plasma conditions (refer to Figure 5) of $\dot{m}_p = 5$ sccm (a), $\dot{m}_p = 10$ sccm (b), $\dot{m}_p = 20$ sccm (c). The vertical line at $Z = 10$ mm, identifies the edge of the collimator. The trajectory in dashed red identifies the limit case for ion collection, Y_{lim}.

DOI: 10.13009/EUCASS2023-707

in Figure 5. The low ion kinetic energies involved if compared to the plasma potential, make it easy for the sheath to deflect ions in the direction perpendicular to the surface. The ions within a limit perpendicular distance from the surface Y_{lim} would end up colliding with the surface (collimator) and be neutralized. Y_{lim} thus depends on the combination of ion energy, and electric field E_Y. It is found that Y_{lim} = 2.6 mm, 3.45 mm, and 3.17 mm, for 5, 10, and 20 sccm respectively. Note that the ions at a sufficiently large distance from the surface will stay unaffected and continue traveling in the z direction as the perpendicular electric field decreases.

Although involving several important assumptions, this simple model is able to show that a significant part of the probe aperture area is lost because of the formation of a sheath on the surface of the collimator. This sheath is responsible for the collection of part of the ions which are recombined at the collimator surface and are consequently not able to reach any collector.

The ions which are most affected are those traveling in proximity to the collimator surface and consequently are the ones that would have most probably been collected by the lateral collector. In this regard, the reduced I_L current collected by FC-B (refer to 8-b), suggests that this effect is larger for the continuous collimator (C2). Neglecting 2D boundary effects between the disks composing C1, it is expected that this effect is substantially lower for this electrode since each disk is only 1.5 mm thick. On the other hand, both collimators are axially symmetric, which results in a null radial electric field at the axis. Thus, ions traveling in proximity to the axis will proceed unaffected by the sheath formation and collide with the back collector. This consideration is in agreement with the small difference between the current collected on the back collector by the two probes.

On a final note, the Y_{lim} found for the three mass flow rates shows that the ions are less affected by the sheath at 20 sccm with respect to the 10 sccm cases. As $\dot{m}_p$ increases the electron temperature decreases and the density increases, both effects reduce the Debye length $\lambda_D \propto \sqrt{\frac{T_e}{n_e}}$, hence tending to lower Y_{lim}. However, as seen in Figure 5-a the ion energy is reduced with $\dot{m}_p$, making the ions easier to be deflected (tendency to enlarge Y_{lim}). Hence, the decreased Y_{lim} for 20 sccm if compared with the 10 sccm case, can be explained by the slower decrease in ion energy with $\dot{m}_p$ with respect to Debye length. This phenomenon increases the effective aperture area, possibly explaining the reduced disagreement between FC1 and FC2 observed at 20 sccm as seen in fig 8-b and c.

4.3 Effect of the collector length

The length of the collector in a Faraday Cup is thought to be associated with the probe's capability of recollecting secondary electrons emitted by ions impacting the electrode surface [10]. Furthermore, as mentioned in Section 3.1, the design of a FC should take into account the Child-Langmuir sheath expansion due to the applied voltage bias. Hence, in both cases, probes that are too short may affect the accuracy of the ion current measurement, either by losing the capability of recollecting SEE or by perturbing the external plasma respectively. The effect of the collector length has been tested by using the FC-A and C. Being FC-A equipped with a 4 cm long collector, and FC-C with a 2 cm collector. Both probes implement the split aluminum collector design.

Figures 10-a and b, show the collected currents at 5 sccm for the two probes FC-A and FC-C as an illustrative case. Firstly, the two probes collect the same amount of total ion current I_T, both at $\alpha = 0°$ and 60°. As visible in Figure 10-c, this is true also for 10 and 20 sccm, being the disagreement in the same order of the current variation due to the thruster repeatability ($\approx 5\%$). On the other hand, FC-A and FC-C show a clear difference in how I_T is distributed between the lateral and back collector. This is expected since the "field of view" of the back collector is larger for the 2 cm design, being closer to the collimator/probe aperture with respect to the 4 cm case. Moreover, while the total current is close to constant, the ratio of current I_L/I_B decreases for both probes with increasing $|V_b|$. This is more evident for probe FC-C where the ratio becomes lower than 1 for the 5 sccm case. A possible interpretation of this exchange of current between the lateral and the back collector might be linked to the shape of the iso-potential surfaces within the collector. As the applied negative bias potential increases, creating a thicker Child-Langmuir sheath, the iso-potential lines may become from concave (following the collector curvature) to flatter. The resulting electric field would affect the ion trajectory deviating the ions that were collected by the lateral collector at low $|V_b|$ towards the back collector.

DOI: 10.13009/EUCASS2023-707

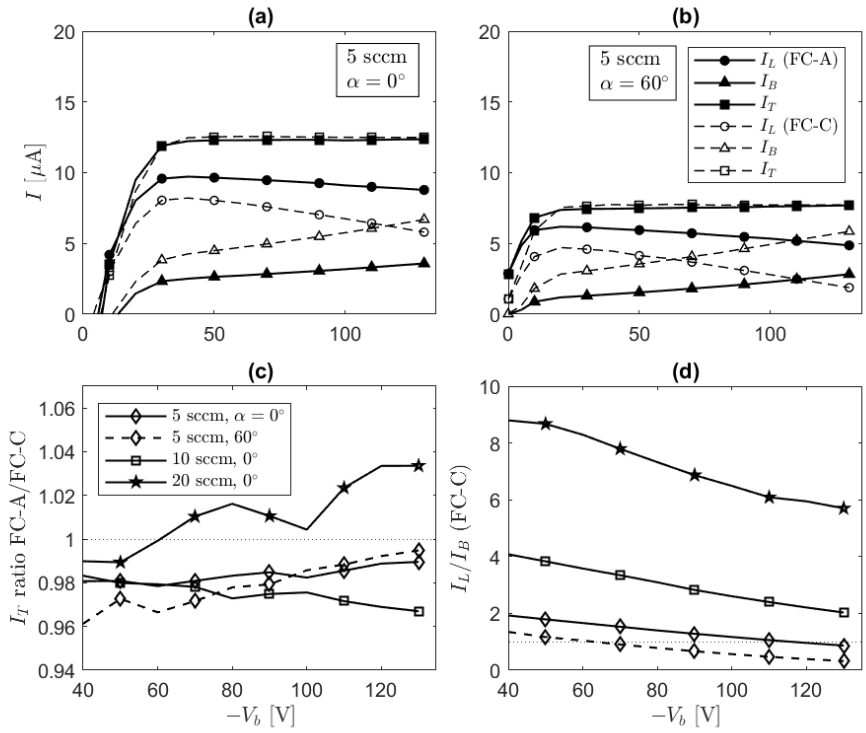

Figure 10: (a-b) Ion currents collected at 5 sccm respectively for $\alpha = 0°$(a) and $\alpha = 60°$(b) for FC-A (solid line) and FC-C (dashed line). (c) Ratio of total current collected between the 4 and 2 cm probes. (d) Ratio of lateral to back collected current from the 2 cm probe (FC-C).

The case at 5 sccm, at $\alpha = 60°$ (Figure 10-b) offers the possibility of having a similar ion energy to $\alpha = 0°$, but with lower density (refer to 5-a and b). For this case, the effect is accentuated because of the increased characteristic sheath size within the probe. Hence, further decreasing the collector length, might be detrimental since the iso-potential lines could become convex and possibly affect the ion collection at low densities. However, conducting a non-quasi-neutral plasma simulation, similar to those carried out for the RPA case by Cichocki et al.[21], would help verify these hypotheses by solving the potential distribution inside the probe under various measurement conditions.

4.4 Effect of the Collector material

Probe configurations FC-C and FC-D were used to test if the collector material has any influence on the ion current collection accuracy. For this purpose, the material of the back collector for FC-D has been chosen to be tungsten, which is expected to provide a lower SEE yield [22, 3]. Note that the collector length for this comparison has been chosen to be 20 mm since it shows a lower I_L/I_B, hence any effect inherent to the SEE from the back electrode would be accentuated and easier to be clearly identified.

Figure 11 shows the relative difference between the total current collected by the two probes, with respect to the probe FC-C. Also for this scenario, small variations in I_T were observed, the current collected by FC-D is ± 1-4% lower than FC-C. However, this variation is small, being in the same order as the uncertainty on the repeatability of ion current measurements for successive firings of the Helicon thruster, concluding that if there is any SEE effect, this is small and can be disregarded. A similar result was also obtained by Engelman with a molybdenum collector [23].

DOI: 10.13009/EUCASS2023-707

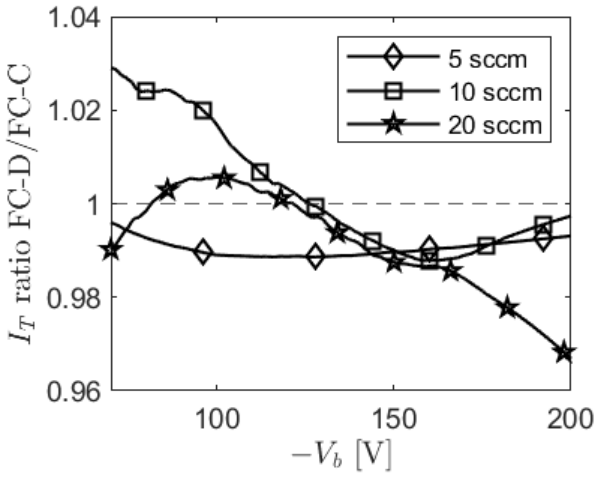

Figure 11: Ratio between the total current I_T collected by FC-D (Back collector in Tungsten) and FC-C (Back collector in Aluminium).

Finally, the fact that the I_T current collection is insensitive to the probe length used in this study (20-40 mm long) and collector material (aluminum vs tungsten) points out that SEE generation or non-recollection of SEE could be a negligible effect in the range of ion energies used in this study.

5. Conclusions

A novel modular Faraday Cup prototype has been developed to identify the effects of several design parameters on the ion current measured. The impact of two types of collimator shapes (C1 and C2), collector length (4 and 2 cm long), and collector material (Aluminium and Tungsten) were analyzed. As a further diagnosing tool, the collector used is segmented into two parts (the lateral and back collector). This expedient made it possible to provide insights into the ion current distribution within the probes.

Auxiliary experimental data characterizing the plume of the thruster were obtained with a LP and an RPA. The resulting current density estimations obtained from the data they provided on the axis exhibit a promising agreement with those derived from FC-A. On the other hand, the probe equipped with the C2 collimator always showed about 50% less collected current with respect to the probe with C1. The measurements with the segmented collector allowed checking that the source of the current discrepancy is the lower amount of ions reaching the lateral collector. A simple 1D model of an electrostatic sheath has been proposed to explain the ion optics around the collimator region. It showed that the trajectory of the ions is curved towards the collimator by the electric field arising within the sheath. The ions are recombined at that wall, preventing them from being collected by the collector. This effect is expected to be stronger for C2 with respect to C1 because of its shape. Suggesting that thin collimators might be a better option. This phenomenon is expected to mainly affect the current collection on the lateral collector, in agreement with the experimental data.

Both the collector length and material were expected to influence secondary electron emission by ion impact. However, the proposed experiments have demonstrated that the variation in the total collected ion current among the tested probes is minimal. This suggests that, under the plasma conditions involved in this study, SEE emission and their recollection are not influenced by the probe's length or material. As a speculation, this lack of effect could be attributed to the low presence of secondary electrons under the tested conditions.

Furthermore, the study on the probe length has revealed that probes shorter than 2 cm could potentially disturb the upstream plasma in the low-density regions, thereby affecting the collection of ion current.

Although multiple parameters were investigated, it is not possible with the current experimental setup to evaluate the absolute accuracy of the probes on the ion current measured, since the total plume current is not known a priori: i.e. other design parameters might exist which could have a significant effect on the ion current collection, such as ion optics phenomena derived by border effects on the collimators or the diameter of the collector.Thus, to fully address the optimal probe design for a FC for electrodeless plasma thrusters, 2D axisymmetric plasma simulation should be carried out to highlight any further phenomenon happening within the probe. Concurrently, an experimental calibration of the probes should be performed with a source providing a known current and with ions in comparable energy and density ranges as those in this study. This would ease probe design iterations and increase measurement accuracy.

DOI: 10.13009/EUCASS2023-707

6. Acknowledgments

This work has been supported by the European Space Agency, under contract 4000133612/21/NL/RA. Additional funds come from the project SUPERLEO, TED2021-132484B-I00, financed by the Agencia Estatal de Investigación of Spain.

References

[1] SN Bathgate, MMM Bilek, and DR Mckenzie. Electrodeless plasma thrusters for spacecraft: a review. *Plasma Science and Technology*, 19(8):083001, 2017.

[2] Eduardo Ahedo. Plasmas for space propulsion. *Plasma Physics and Controlled Fusion*, 53(12):124037, 2011.

[3] S Mazouffre, G Largeau, L Garrigues, C Boniface, and K Dannenmayer. Evaluation of various probe designs for measuring the ion current density in a hall thruster plume. In *35th International Electric Propulsion Conference*, number IEPC-2017-336, 2017.

[4] Daniel L Brown and Alec D Gallimore. Evaluation of ion collection area in faraday probes. *Review of Scientific Instruments*, 81(6), 2010.

[5] Daniel L Brown, Mitchell LR Walker, James Szabo, Wensheng Huang, and John E Foster. Recommended practice for use of faraday probes in electric propulsion testing. *Journal of Propulsion and Power*, 33(3):582–613, 2016.

[6] M.L.R. Walker, R.R. Hofer, and A.D. Gallimore. Ion collection in Hall thruster plumes. *Journal of Propulsion and Power*, 22(1):205, 2006.

[7] E Cantero, D Lanaia, M Fraser, A Sosa, E Bravin, D Voulot, and W Andreazza. Performance tests of a short faraday cup designed for hie-isolde. Technical report, 2013.

[8] Smruti Ranjan Mohanty, Heman Bhuyan, Nirod Kumar Neog, Rabindra Kumar Rout, and Eiki Hotta. Development of multi faraday cup assembly for ion beam measurements from a low energy plasma focus device. *Japanese journal of applied physics*, 44(7R):5199, 2005.

[9] J Prokpek, J Kaufman, D Margarone, M Krs, A Velyhan, J Krása, T Burris-Mog, S Busold, O Deppert, TE Cowan, et al. Development and first experimental tests of faraday cup array. *Review of Scientific Instruments*, 85(1), 2014.

[10] Valentin Hugonnaud, Stéphane Mazouffre, and David Krejci. Faraday cup sizing for electric propulsion ion beam study: Case of a field-emission-electric propulsion thruster. *Review of Scientific Instruments*, 92(8), 2021.

[11] Hugonnaud Valentin and Mazouffre Stéphane. Optimization of a faraday cup collimator for electric propulsion device beam study: Case of a hall thruster. *Applied Sciences*, 11(5):2419, 2021.

[12] J Navarro-Cavallé, M Wijnen, P Fajardo, and E Ahedo. Experimental characterization of a 1 kw helicon plasma thruster. *Vacuum*, 149:69–73, 2018.

[13] V. Gómez, A. Giménez, M. Ruiz, J. Navarro-Cavallé, P. Fajardo, M. Wijnen, and E. Ahedo. Rf power-plasma coupling experimental results in a helicon plasma thruster prototype. In 36^{th} *International Electric Propulsion Conference*, number IEPC-2019-365, Vienna, Austria, 2019. Electric Rocket Propulsion Society.

[14] AE Vinci, Stéphane Mazouffre, Marco R Inchingolo, Víctor Gómez, Pablo Fajardo, and Jaume Navarro-Cavallé. Probing xenon atoms and ions velocity in the magnetic nozzle of a helicon plasma thruster. In *37th International Electric Propulsion Conference*, 2022.

[15] Mick Wijnen. *Diagnostic Methods for the Characterization of a Helicon Plasma Thruster*. PhD thesis, Universidad Carlos III de Madrid, Leganés, Spain, 2022.

[16] Robert B. Lobbia and Brian E. Beal. Recommended practice for use of langmuir probes in electric propulsion testing. *Journal of Propulsion and Power*, 33(3):566–581, 2017.

[17] Kristi de Grys, Dennis Tilley, and Randy Aadland. Bpt hall thruster plume characteristics. In *35th Joint Propulsion Conference and Exhibit*, page 2283, 1999.

DOI: 10.13009/EUCASS2023-707

[18] Richard R Hofer, Mitchell LR Walker, and Alec D Gallimore. A comparison of nude and collimated faraday probes for use with hall thrusters. In *27th International Electric Propulsion Conference*, pages 01–020. Electric Rocket Propulsion Soc. Fairview Park, OH, 2001.

[19] M. R. Inchingolo, M. Merino, and J. Navarro-Cavallé. Plume characterization of a waveguide ecr thruster. *Journal of Applied Physics*, 133(11):113304, 2023.

[20] Jaume Navarro-Cavallé, Mick Wijnen, Pablo Fajardo, Eduardo Ahedo, V. Gómez, A. Giménez, and M. Ruiz. Development and characterization of the helicon plasma thruster prototype hpt05m. In 36th *International Electric Propulsion Conference*, number IEPC-2019-596, Vienna, Austria, 2019. Electric Rocket Propulsion Society.

[21] Filippo Cichocki, Jaume Navarro-Cavallé, Alberto Modesti, and Gonzalo Ramírez Vázquez. Magnetic nozzle and rpa simulations vs. experiments for a helicon plasma thruster plume. *Frontiers in Physics*, 10, 2022.

[22] Homer D Hagstrum. Auger ejection of electrons from tungsten by noble gas ions. *Physical Review*, 96(2):325, 1954.

[23] S.F. Engelman and J.M. Fife. Hemispherical measurements of the spt-140 plume. Technical report, 2002.